# CURRENT PROFILE MODIFICATION WITH ELECTRON CYCLOTRON CURRENT DRIVE IN THE DIII–D TOKAMAK*

T.C. LUCE, Y.R. LIN-LIU, J.M. LOHR, C.C. PETTY, R. PRATER, R.W. CALLIS, J.S. deGRASSIE, R.I. PINSKER, D. PONCE
DIII–D National Fusion Facility, General Atomics, San Diego, California 92186-5608

M.E. AUSTIN
University of Texas at Austin, Austin, Texas

F.W. BAITY, Jr., M. MURAKAMI
Oak Ridge National Laboratory, Oak Ridge, Tennessee

S. BERNABEI, K.-L. WONG
Princeton Plasma Physics Laboratory, Princeton, New Jersey

G. GIRUZZI
Association EURATOM-CEA, Centre d'Etudes Nucleaires de Cadarache, Cadarache, France

R.W. HARVEY
CompX, Del Mar, California

B.W. RICE
Lawrence Livermore National Laboratory, Livermore, California

M. ZERBINI
ENEA, Magnetic Confinement Fusion Physics, Rome, Italy

**Abstract**

Proof-of-principle experiments on the suitability of electron cyclotron current drive (ECCD) for active current profile control are reported. Experiments with second harmonic extraordinary mode absorption at power levels near 1 MW have demonstrated ability to modify the current profile. This modification is manifested in changes in the internal inductance and the time at which sawteeth appear. Measurements of the local current density and internal loop voltage using high resolution motional Stark effect spectroscopy to half of the minor radius in discharges with localized deposition clearly demonstrate localized off-axis ECCD at the predicted location. Comparison with theory indicates the detrimental effect of trapped electrons on the current drive efficiency is less than predicted. Modification of the theory for finite collisionality is the leading candidate to explain the observations.

## 1. INTRODUCTION

Control of the plasma current profile is necessary to extend the high performance discharges observed on the DIII–D tokamak and other tokamaks to steady state. Beyond the obvious need to maintain the total plasma current non-inductively, both the stability of the plasma and the transport of energy across the magnetic field depend on the current profile. Electron cyclotron current drive (ECCD) is a leading candidate to fulfill the role of plasma current profile control due to the straightforward ability to control the location and the magnitude of the non-inductive current under a wide variety of conditions, and the absence of the technical complication of plasma-antenna interactions.

The present system for ECCD on the DIII–D tokamak consists of two gyrotrons operating at 110 GHz. The system and verification of its proper operation have been described in detail elsewhere [1,2], so only a brief description will be given here. The two gyrotrons are rated for 0.9 MW for 2 s and 0.8 MW for 1 s, respectively. The pulse lengths are currently limited by heating of the gyrotron output window, but are adequate for the present proof-of-principle experiments. The power is transmitted via evacuated corrugated waveguide (31.75 mm diam) to the tokamak. Each transmission line contains a pair of miter bends which use grooved mirrors to set almost any desired polarization.

*Work supported by U.S. Department of Energy under Contracts DE-AC03-89ER51114, DE-AC05-96OR22464, DE-AC02-76CH03073, W-7405-ENG-48, and Grant No. DE-FG03-96ER54373.

Two separate launcher assemblies, neither of which have a vacuum window, have copper mirrors which can steer the beam poloidally. The toroidal angle is fixed in each launcher — either for co-current drive ($\phi$ = 24°–31° depending on the poloidal angle) or for nearly radial launch, which allows heating without current drive. All of the results reported here use the co-current drive launcher. A vacuum opening of the transmission line is required to switch between launchers, so comparison of co-current drive with pure heating is not possible in a single day. The experiments reported here all employ second harmonic absorption of the extraordinary-mode polarization. Polarization purity and deposition location experiments have been successfully carried out [1,2]. As a whole, the ECCD system has a demonstrated reliability comparable to the neutral beam systems on DIII–D.

The results reported here represent the proof-of-principle phase of a program to implement an active current profile control system on the DIII–D tokamak. Three key elements of the proof-of-principle are presented here. First, the ability to modify the current profile by varying the deposition location is demonstrated by changes to global quantities related to the current profile such as the internal inductance ($\ell_i$) and the appearance of MHD instabilities identified with the q=1 surface such as sawteeth or m=1/n=1 modes. Second, localized current drive is measured by means of an analysis technique which makes use of the unique diagnostic capabilities of the DIII–D tokamak. While central current drive has been previously measured on DIII–D, the first quantitative measurement of localized off-axis ECCD in any toroidal device is reported here. Third, these current drive measurements are compared with various theoretical calculations in order to validate a predictive model of ECCD.

The discharges for the study of ECCD utilize early neutral beam injection (NBI) to delay the onset of sawteeth by raising the electron temperature ($T_e$) and to allow continuous measurement of the internal magnetic fields by means of motional Stark effect (MSE) spectroscopy [3]. This enables detailed reconstruction of the magnetic equilibrium with the EFIT code [4]. An example of the effect of central ECCD is shown in Fig. 1. A single gyrotron is pulsed on at 1.5 s. The time sequence of equilibria show that the $\ell_i$ and central safety factor q(0) deviate significantly from the NBI-only fiducial. While central heating should eventually have a similar result, the time scale for current penetration should be longer, not shorter, if this were a pure heating effect. The time history of the central poloidal flux $\psi(0)$

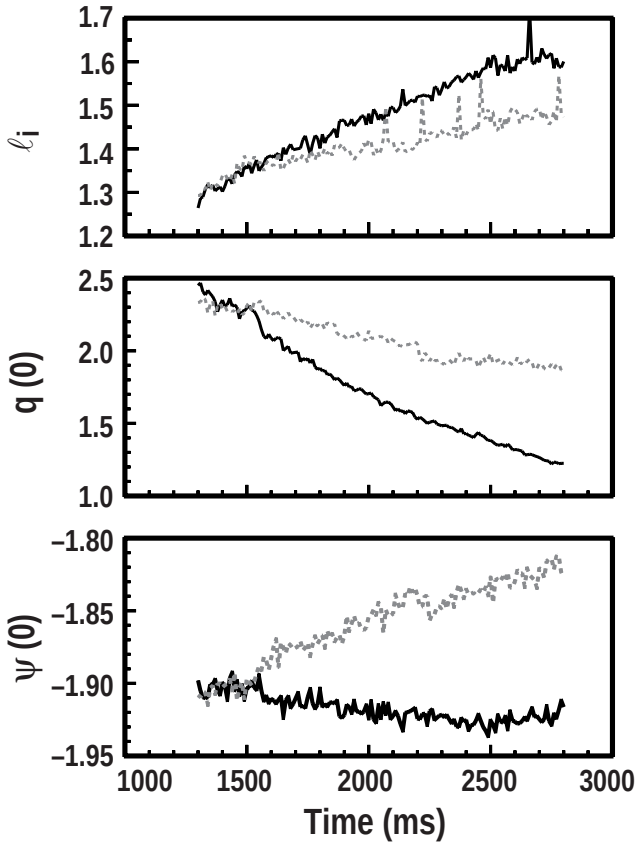


*FIG. 1. Time histories of the internal inductance $l_i$, the central safety factor q(0), and the poloidal flux at the magnetic axis $\psi(0)$ for discharges with ECCD (solid line) and without (dashed line). A single gyrotron delivers ~0.5 MW starting at 1.5 s.*

also directly indicates that non-inductive current is the cause of the peaking. The time derivative of the poloidal flux is the local loop voltage, and the case with ECCD has a negative voltage indicating a non-inductive current source greater than the total existing current density on axis.

Another indication of current profile modification is the timing of the appearance of a q=1 surface in the plasma as evidenced by the onset of sawteeth or m=1/n=1 modes. For current drive on-axis, the q=1 surface should appear more quickly than in the fiducial case since current is being supplied more rapidly than is possible by diffusion. In the case of weak off-axis current drive, the current profile is broadened and less inductive flux is required which together delay the appearance of the q=1 surface. Evidence of these effects is shown in Fig. 2. The top part of the figure shows time histories of central

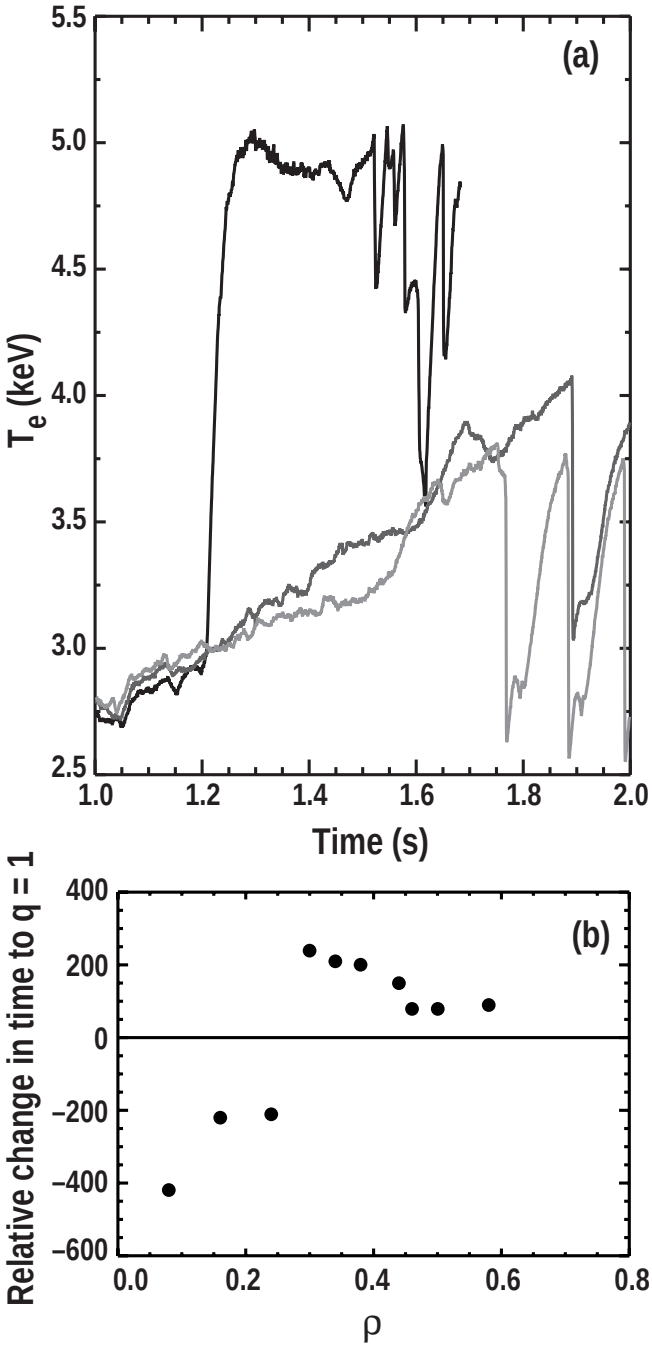


*FIG. 2. (a) Time histories of central electron temperature. The first sharp drop in temperature in each trace signifies the time of the first sawtooth. The central ECCD case has the first sawtooth at 1.52 s while the off-axis case has the first sawtooth at 1.89 s. The NBI-only fiducial case has the first sawtooth at 1.74 s. Note that the sawteeth are also much more rapid in the central ECCD case. (b) A dataset of similar discharges (same q, density, and ECH power) showing the effect illustrated in (a) is systematic. Current drive inside of ρ = 0.3 hastens the onset of sawteeth while current drive for ρ > 0.3 delays the onset of sawteeth as discussed in the text.*

$T_e$ for three cases: NBI-only, ECCD at $\rho = 0.2$, and ECCD at $\rho = 0.45$. (The coordinate $\rho$ is the square root of the normalized toroidal flux normalized to the edge value which acts as a relative radial coordinate.) In the off-axis case, the first sawtooth crash is delayed by more than 0.1 s, while central case induces the first sawteeth over 0.2 s earlier, despite the significant rise in $T_e$. The lower part of the figure shows the change in the time at which a q=1 surface appears, relative to a NBI-only fiducial with equal plasma current (I) and toroidal field (B), as a function of deposition radius. The datasetconsists of ten discharges with equal injection power ($P_{EC}$) and electron density (n). The systematic trend discussed above is apparent and the magnitude of the effect appears consistent with the magnitude of the driven current, which drops with radius due to the lower local $T_e$. The conclusion is that the ECCD is capable of making measurable modifications of the current profile over the range of radius where experiments were carried out ($\rho = 0.1$–$0.6$). This sets the stage for the next step, which is to quantify the location and magnitude of the ECCD.

Measurement of the non-inductive current profile in the absence of resistive equilibrium requires simultaneous knowledge of the current density profile and the internal electric potential or loop voltage (V). These quantities are inferred on DIII–D by calculating the poloidal flux $\psi$ on a spatial grid as a function of time [5]. The high spatial resolution measurements of the internal magnetic fields by MSE are necessary to provide the required accuracy and resolution. Two spatial derivatives of $\psi$ give the total current density while the time derivative of $\psi$ at constant $\rho$ gives the loop voltage at that surface. Using a neoclassical conductivity [6], the non-inductive current density ($J_{NI}$) is given by the difference of the total current density ($J_{||}$) and the inductive current density ($J_{OH} = \sigma E_{||}$). The remaining$J_{NI}$ is a combination of NB, bootstrap, and EC current. To isolate the ECCD, an NBI-only fiducial is prepared identically to the ECCD shot, and the difference is formed. This difference iscorrected for the change in kinetic parameters between the two shots, but that correction is usually small. The assumptions of neoclassical resistivity and bootstrap current have been validated experimentally [5].

Two examples of off-axis ECCD analyzed by this technique are shown in Fig. 3. The left-hand column shows a case with deposition at $\rho = 0.2$ and the right-hand column shows a case with $\rho = 0.45$. Starting with the left-hand case, the top figure shows $J_{||}$ from the equilibrium reconstruction for the ECCD and NBI-only cases. Notice that in the 0.5 s since the turn-on of the ECCD, the current profile has been substantially modified in agreement with the discussion above of Fig. 2. This magnitude of change is consistent with resistive simulations. The next box down shows the inferred loop voltage as a function of radius for both cases. The error bars are the random errors arising from fitting the time series of equilibria. This is estimated to be the dominant source of random error in this calculation and is propagated throughout the remaining calculations. As explained above, the neoclassical conductivity is calculated from the measured n, $T_e$, and impurity concentration ($Z_{eff}$) and combined with V and $J_{||}$ to give $J_{NI}$ (third box). (The graph ends at $\rho = 0.7$ because no $Z_{eff}$ measurements are available outside of this.) Finally, the difference in the non-inductive current between the ECCD and fiducial shot is shown in the bottom box. This difference is ascribed to ECCD. The integrated difference current out to $\rho = 0.4$ is 48 kA. The apparent current for $\rho > 0.4$ is ~10 kA and is likely due to the accumulation of the systematic errors of this technique. While the accumulated random error in the driven current is large (~34 kA), making definitive comparisons at that level difficult, the peak current density is >2 standard deviations (2 $\sigma$) from 0, and the peak is clearly resolved to better than 1 $\sigma$.

The right-hand column represents a case with the beam steered to $\rho = 0.45$. In this case, no significant change in $J_{||}$ is observed after 0.5 s (top box), but the ECCD is revealed by the reduction in V required locally to drive the same current (second box). The difference in non-inductive current appears at the expected location and is reduced in magnitude from the $\rho = 0.2$ case (third and fourth boxes). The peak is resolved to 1 $\sigma$ and is >2 $\sigma$ from 0. The driven current in the positive peak is 31 kA. These cases are typical of the presently analyzed dataset in that the inferred peak current density appears at the expected location within the systematic errors of the aiming calibration, and the peak current density is significantly above any systematic or random errors apparent in the data.

The combination of poloidal beam steering and variation in the toroidal field allows assessment of the effects of trapped electrons on the ECCD. Two types of scans have been analyzed using the current drive analysis technique described above. The first is a scan of poloidal position at fixed toroidal field such that the resonance intersects the magnetic axis. The second type is a correlated variation of B and poloidal aiming to scan the poloidal deposition location at fixed $\rho$. In varying B, the plasma current is varied proportionately to keep the q profile similar, in order to avoid any difficulties with MHD instabilities. This dataset was obtained with roughly constant line-averaged electron density ($1.7$–$1.8\times10^{13}$ cm$^{-3}$) and $P_{EC}$ (0.95–1.14 MW). The figure of merit chosen to evaluate these scans is the local current drive efficiency $\eta$ ($\equiv nI_{EC}R/P_{EC}$, with n the density at the deposition location and

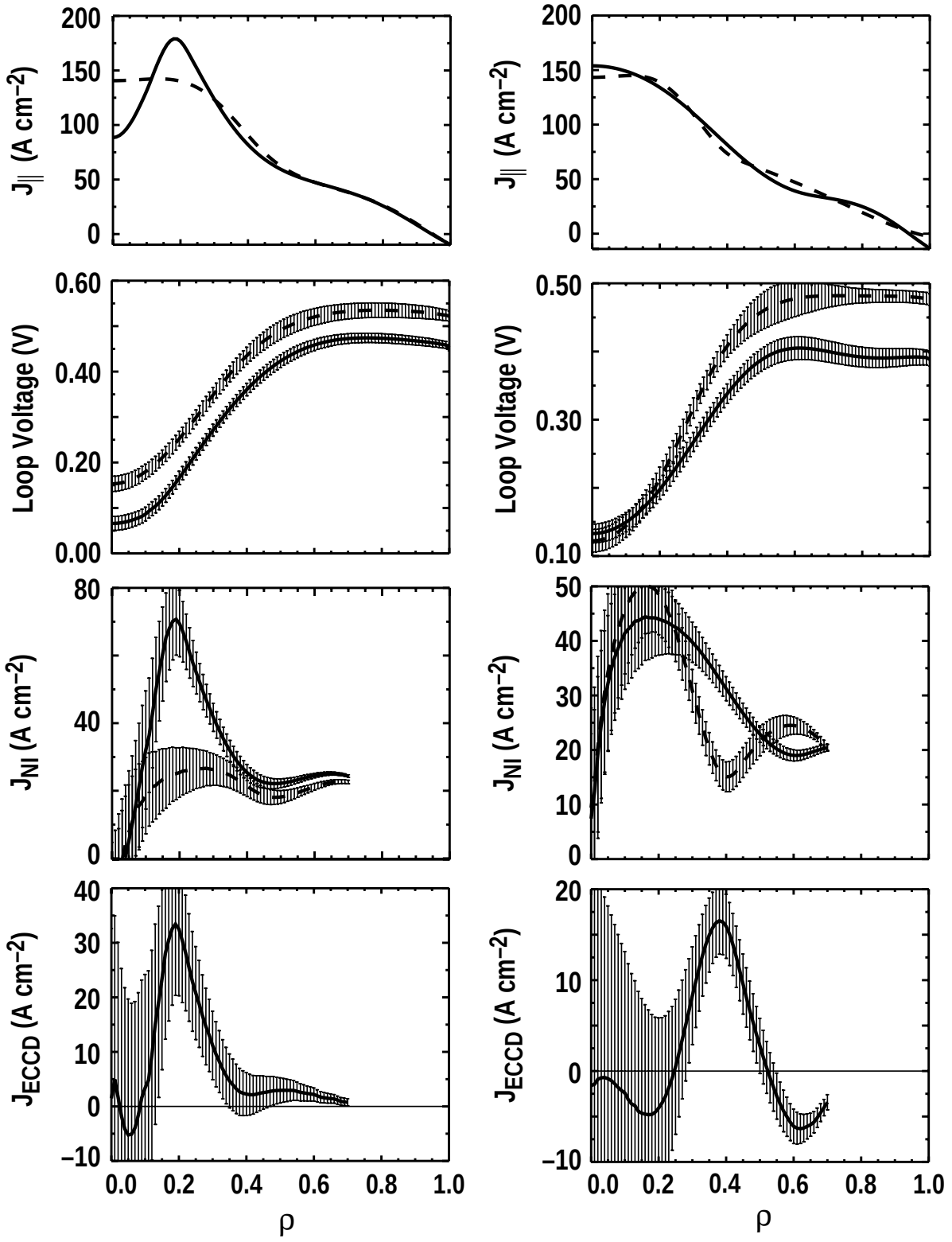


*FIG. 3. Measurements of the current density due to the ECCD. The left column is analysis of a case with the beam aimed at $\rho = 0.2$. The plasma parameters in the ECCD discharge are B = 1.97 T, I = 0.98 MA, $\bar{n} = 1.7\times10^{13}$ cm$^{-3}$, $P_{EC} = 1.03$ MW. The right column is analysis of a case with the beam aimed at $\rho = 0.4$. The plasma parameters in the ECCD discharge are B = 1.76 T, I = 0.89 MA, $\bar{n} = 1.8\times10^{13}$ cm$^{-3}$, $P_{EC} = 1.14$ MW. The solid lines are the ECCD discharge in each case and the dashed lines are the NBI-only fiducial discharge. The top box is the total current density, the next box is the loop voltage, the third box is the non-inductive current density, and the bottom box is the ECCD current density. All traces are plotted versus the radial coordinate $\rho$.*

the major radius of the center of the flux surface where the current is driven) normalized by the theoretically expected linear temperature dependence. The radial scan shown in Fig. 4 indicates that the normalized efficiency $\eta/T$ is independent of $\rho$ in the region where experiments were carried out ($\rho$ = 0.1–0.5). Note that the driven current does drop over this range; it is only the normalized efficiency which is constant. This lack of dependence on $\rho$ is in contrast to the theoretical results also illustrated in Fig. 4. Three types of calculations are displayed in the figure — a linear calculation [7], a quasi-linear Fokker-Planck calculation [8], and a quasi-linear Fokker-Planck calculation with the effects of $E_{||}$. The Fokker-Planck calculations have been verified with an independent code [9]. With the exception of the centermost case where the high power density results in a significant quasi-linear effect, the three calculations obtain roughly the same answers. Since the ffective trapped particle fraction rises by approximately a factor of 2 over this range of $\rho$, it appears that the normalized efficiency does not depend as strongly on this quantity as predicted by theory.

This same conclusion is consistent with the results of the poloidal location scans shown in Fig. 5. At both $\rho$ = 0.35 and $\rho$ = 0.45, the normalized efficiencies are well above the theoretical predictions, indicating that the effect of trapped electrons is significantly less than predicted. The effect of trapped electrons is not completely absent as shown by points in the figure which represent calculations of the ECCD in the absence of trapped particles. The poloidal variation in both scans is due in part to the local trapped particle fraction change and in part due to the upshift of the toroidal index of refraction due to damping at small major radius. The relative importance of these two effects is being investigated.

One possible explanation for the weaker trapped electron effect is modification of the trapped particle boundary by finite collisionality. The theoretical calculations applied to the scans in Figs. 4 and 5 all impose a trapped particle boundary assuming zero collisionality, i.e., a boundary which continues down to zero velocity. In the trapped particle region of velocity space, the characteristic time is the bounce time, which is assumed in these calculations to be much shorter than the pitch-angle scattering time characteristic of the passing region. Therefore, electrons which diffuse into the trapped particle region from the co-current side emerge rapidly (compared to the pitch-angle scattering time) on the counter-current side. This is the Ohkawa effect [10]. Finite collisionality reduces the size of the trapped region roughly in proportion to $\sqrt{\nu_*}$, and reduces it preferentially at low velocity. This has the somewhat surprising result that finite collisionality increases the net current, because electrons

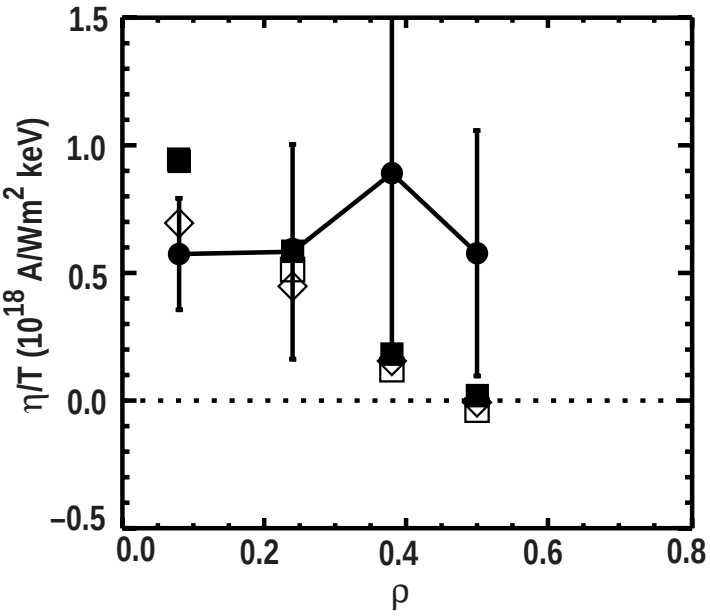


*FIG. 4. Comparison of experimental and theoretical current drive efficiency normalized to temperature. The experimental efficiency (circles) is roughly independent of radius while the theoretical efficiencies drop sharply with increasing radius. Three theoretical calculations are shown: linear theory (diamond), quasi-linear Fokker-Planck calculation (open square), and Fokker-Planck with parallel electric field (filled square).*

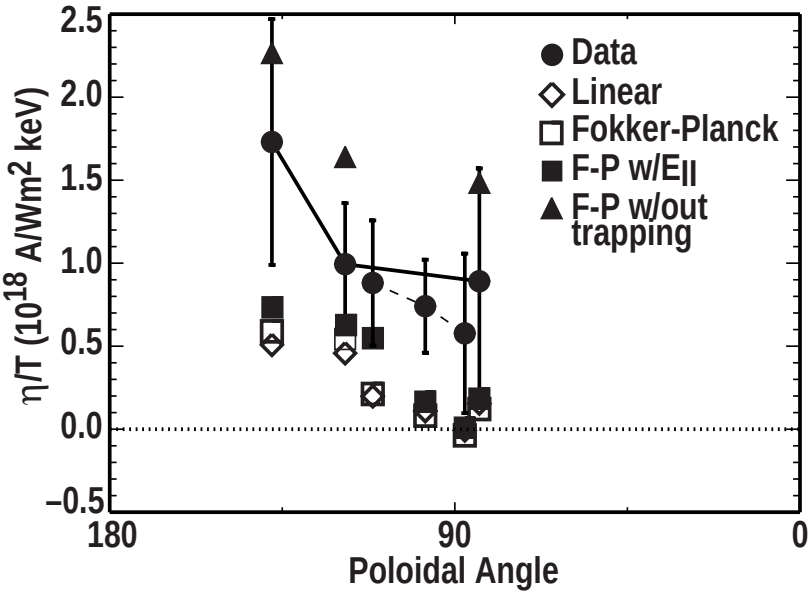


*FIG. 5. Variation of normalized efficiency with poloidal angle at fixed ρ. The points connected by the solid line are ρ = 0.30–0.38. The points connected by the dashed line are for ρ = 0.44–0.50. Poloidal angle is defined as the angle with respect to the major radius with the magnetic axis as the origin. The outboard midplane is the 0° reference, vertically above the axis is 90°, and the inboard midplane is 180°.*

spend more time on the co-current side of the distribution. The data in Fig. 5 lie between the calculations with zero collisionality and the calculations with no trapped particles, which indicates that a reduction of the trapped particle region can explain the data. A predictive model based on finite collisionality theory has not yet been developed.

A qualitative assessment of the implications of this effect for ECCD on DIII–D and future devices can be made. The discharges reported here have the same collisionality as envisioned for high fusion power devices such as ITER [11]. However, the plasma β is significantly lower than planned for these discharges. The effect of higher β is to move the wave-particle interaction to higher velocity where the finite collisionality effects are small and to higher parallel velocity (due to relativistic effects) where the distance to the trapped particle region is larger. Therefore, the observed enhancements in the DIII–D experiments should be less significant in next step devices, The same argument is true for the advanced tokamak discharge scenarios for DIII–D which have higher β and lower collisionality than these proof-of-principle discharges. Using the same zero collisionality calculations as referenced above, substantial off-axis current is predicted at the half radius in these scenarios, due to the higher β.

With the present 1 MW ECCD system on DIII–D, it has been possible to modify the current profile evolution and make clear measurements of localized off-axis ECCD. The measured off-axis current drive efficiencies are higher than predicted, indicating that some refinement of the theory is necessary. This work supports the development of the 6 MW ECCD system planned for completion in 2000 as an active current profile control tool for the DIII–D tokamak.

REFERENCES

[1] CALLIS, R.W., *et al*., Proc. 20th Symposium on Fusion Technology, Vol. I (1998) p. 315.
[2] LOHR, J., *et al*., Proc. 23rd Int. COnf. Infrared and Millimeter Waves (1998) p. 269.
[3] RICE, B.W., *et al*., Phys. Rev. Lett. **79**, 2694 (1997).
[4] LAO, L.L., *et al*., Nucl. Fusion **30**, 1035 (1990).
[5] FOREST, C.B., *et al*., Phys. Rev. Lett. **73**, 2244 (1994).
[6] HIRSHMAN., S.P., Phys. Fluids **31**, 3150 (1988).
[7] COHEN, R.H., Phys. Fluids **30**, 2442 (1987).
[8] HARVEY, R.W., McCOY, M.G., in Advances in Simulation and Modeling of Thermonuclear Plasmas (Proc. IAEA Tech. Comm. Mtg, Montreal, 1992), IAEA, Vienna (1993), p. 498.
[9] GIRUZZI, G., Phys. Fluids **31**, 3305 (1988).
[10] OHKAWA,T., General Atomics Report GA–A13847 (1976).
[11] PETTY, C.C., *et al*., Phys. Plasma **2**, 2342 (1995).